

Resolvent methods for steady premixed flame shapes governed by the Zhdanov-Trubnikov equation

Gaëtan Borot

*Section de Mathématiques, Université de Genève,
2-4 rue du Lièvre, 1206 Genève 4, Switzerland.**

Bruno Denet

*Université d'Aix-Marseille, IRPHE, UMR 7342 CNRS, Technopole de Château-Gombert,
49 rue Joliot-Curie, 13384 Marseille Cedex 13, France.†*

Guy Joulin

*Institut P', UPR 3346 CNRS, ENSMA, Université de Poitiers,
1 rue Clément Ader, BP 40109, 86961 Futuroscope Cedex, Poitiers, France.‡*

Using pole decompositions as starting points, the one parameter ($-1 \leq c < 1$) nonlocal and nonlinear Zhdanov-Trubnikov (ZT) equation for the steady shapes of premixed gaseous flames is studied in the large-wrinkle limit. The singular integral equations for pole densities are closely related to those satisfied by the spectral density in the so-called $\mathcal{O}(n)$ matrix model, with $n = -2 \frac{1+c}{1-c}$. They can be solved via the introduction of complex resolvents and the use of complex analysis. We retrieve results obtained recently for $-1 \leq c \leq 0$, and we explain and cure their pathologies when they are continued naively to $0 < c < 1$. Moreover, for any $-1 \leq c < 1$, we derive closed-form expressions for the shapes of steady isolated flame crests, and then bicoalesced periodic fronts. These theoretical results fully agree with numerical resolutions. Open problems are evoked.

PACS numbers: 47.70.Pq ; 47.20.Ky ; 05.20.Jj ; 02.30.Em.

Keywords: Zhdanov-Trubnikov equation ; combustion ; pole decompositions ; resolvents ; random matrices.

I. INTRODUCTION

Most flames propagating into premixed gaseous reactants may be viewed as fronts: their actual thickness $\ell \sim \sqrt{D_{\text{th}} t_{\text{th}}} \sim u_L t_{\text{ch}}$ (based on flat-flame speed u_L , heat diffusivity D_{th} , and chemical time t_{ch}) is often much smaller than the wavelength and amplitude of their deformations. Being also very subsonic (i.e. $u_L \ll$ speed of sound), such combustion fronts border fluids of constant and uniform densities: ρ_u on the fresh side, and $\rho_b < \rho_u$ in the burnt gas. As the Atwood number $\mathcal{A} = \frac{\rho_u - \rho_b}{\rho_u + \rho_b} < 1$ is nonzero, such flames are subject to the hydrodynamic, hence nonlocal, Darrieus [1]-Landau [2] (DL) wrinkling instability at large wavelengths. At shorter scales though, the variations in local normal burning speed u_n (relative to reactants) with front mean curvature [3] bring about a neutral wavelength L_{neutral} proportional to ℓ , yet much longer in practice [4]. Viewing wrinkled flames as fronts embedded in incompressible flows largely facilitates numerical simulations [5] and theoretical analyses thereof.

Acknowledging that $\mathcal{A} \ll 1$ implies a weak DL instability – and hence asymptotically small front slopes and slow evolutions – Sivashinsky analysis [6] provided the first systematic weakly-nonlinear description of the

local amplitude of a wrinkling: a companion numerical work [7] confirmed that the Michelson-Sivashinsky (MS) equation (Eq. (1) with $c = 0$) correctly captures the slow spontaneous dynamics of flat-on-average flames if $\mathcal{A} \rightarrow 0^+$. In physical situations, \mathcal{A} ranges from 0.2 – 0.5 for thermonuclear flames in Supernovae [8] to 0.65 – 0.85 for chemical fronts. It is thus important to incorporate higher orders in \mathcal{A} . The first two subleading orders can be absorbed in a renormalization of coefficients of the MS equation [9–11]. At the third one a new quadratic term in the equation, but the fourth order correction can again be absorbed in coefficients [12]. A similar nonlinearity first appeared in derivations of an equation for the wrinkling amplitude that assumed $\mathcal{A} = O(1)$ and postulated a small flame slope [13, 14].

If a single space coordinate is retained, the Zhdanov-Trubnikov (ZT) type of equation [13] so obtained for slow spontaneous evolutions of front wrinkles reads as follows, in rescaled form:

$$\phi_t + \frac{1}{2}(\phi_x^2 + c\mathcal{H}[\phi_x]^2) = \nu\phi_{xx} - \mathcal{H}[\phi_x], \quad (1)$$

where c is some function of \mathcal{A} , $\phi(t, x)$ is a dimensionless front deformation about a flat shape ($\phi \equiv 0$) ; the subscripts denote derivatives with respect to rescaled time (t) or coordinate (x). For space-periodic cells, $0 < \nu < 1$ will denote the neutral-to-actual wavelength ratio, provided the reference length is suitably chosen. For the isolated crests of infinite wavelengths, $\nu > 0$ could be rescaled to unity by a change of variables but it is kept in (1) for comparisons with cells. The dependence of

* gaetan.borot@unige.ch

† bruno.denet@irphe.univ-mrs.fr

‡ guy.joulin@lcd.ensma.fr

$u_n - u_L$ on curvature gave the $\nu\phi_{xx}$ term in (1), while the Hilbert transform:

$$\mathcal{H}[\phi_x] = \frac{1}{\pi} \int \frac{\phi_x(x') dx'}{x - x'}, \quad (2)$$

in the right-hand side encodes the nonlocal DL instability: a small $\phi(t, x) \propto \exp(\varpi t + i\kappa x)$ indeed has $\varpi = |\kappa| - \nu\kappa^2$ as growth rate. The stabilizing local nonlinearity in (1) combines geometry [6] and hydrodynamics [9]. The nonlocal one, absent from the MS equation ($c = 0$), is mainly fluid-mechanical since $\phi_x^2 + \mathcal{H}[\phi_x]^2$ is proportional to the kinetic energy of wrinkling-induced flow disturbances. It may be destabilizing if $c < 0$, or overstabilizing if $c > 0$, affecting the solutions of (1) in several regards, e.g. at the front tips (local, usually sharp maxima of ϕ).

Besides an interest *per se*, solving the nonlinear and nonlocal (1) analytically with c as general as possible – and viewed here as a free parameter – might help one fit flame shapes from experiments [15]; or from simulations that use $\mathcal{A} = O(1)$ [5]. This could also form the basis of stability analyses of curved fronts, e.g. generalizing that of [16] to large wrinkles. The task is facilitated by the fact that, just like the MS equation [17], (1) where x is replaced by a complex variable $Z = x + iB$, admits meromorphic solutions with pairs of complex-conjugate simple poles $Z_{-k}(t) = Z_k^*(t)$. When restricted to the real line $Z = x$, these solutions are real-valued and represent the front slope. Then, (1) is converted into coupled nonlinear differential equations for the poles $Z_k(t)$ [18]. When the front acquires a steady shape, those poles of ϕ_x that remain at rest for $t \rightarrow \infty$ generically are aligned along parallels to the imaginary axis, due to the same mechanism as for $c = 0$ [17]: at $Z_k = iB_k \pmod{2\pi}$ when x -periodicity is assumed, and also at $Z_m = \pi + iB_m \pmod{2\pi}$ if Neumann boundary conditions are employed (or periodic ones with $x \leftrightarrow -x$ symmetry). In any such steady configurations, the equations that govern the $2N$ motionless pole altitudes may be viewed as expressing an electrostatic (or kinematic) equilibrium under mutual pairwise repulsions between charges (or fluid sources), all subject to an external field originating from the DL instability mechanism. When $N \gg 1$, corresponding to large wrinkles, the spacing between consecutive poles scales like B_N/N , enabling one to adopt a continuous approximation of the equilibrium conditions, and rewrite them as *integral equations for pole densities* [17]. As first shown for $c = 0$ in [19], and confirmed when $c < 0$ [20], a key step to describe the structure of large steady wrinkles is to first solve the simpler case of isolated crests; these have infinite wavelengths and poles at $Z_k = iB_k$ in arbitrary number $2N$.

In [20], such integral equations were solved when $-1 \leq c \leq 0$ by exploiting peculiar properties of index- $\frac{1}{2}$ Meixner-Pollaczek orthogonal polynomials evidenced in [21], firstly for isolated crests and then for monocoalesced periodic fronts (a single maximum of ϕ per wavelength). In both cases, the results nicely agreed with numerical

resolutions of the discrete pole equations when $N \gg 1$. But the naive continuation to $c > 0$ led to unsatisfactory, yet intriguing results. For example, the front slope so obtained for isolated crests with $c > 0$ reads

$$\phi_x(x) = -\frac{1}{\sqrt{c}} \sin \left[\gamma \sinh^{-1} \left(\frac{B_*}{x} \right) \right], \quad (3)$$

with $B_* = \frac{4}{\gamma} \frac{\sqrt{c}}{1-c} \nu N$ and $c = \tanh^2(\pi\gamma/2)$; this lies surprisingly close to the numerically-determined slope profile whenever $0 \leq c \lesssim 0.6$, except very close to $x = 0$ where (3) predicts an essential singularity. The pole density associated with (3) also stays very close to its numerical counterpart, except at $|B| \ll B_*$, where it oscillated infinitely many times and becomes negative at places: this is disallowed, for pole densities must be nonnegative. As conjectured in [20], such localized pathologies might partly result from the failure of an assumption implicitly made in the continuation from $c \leq 0$ to $c > 0$, namely that the density support would still include $B = 0$, instead of being limited to $0 < B_{\min} \leq |B| \leq B_{\max} \approx B_*$ for some $B_{\min} > 0$, and one may imagine that B_{\min}/B_{\max} increases rapidly with c . An analysis of the discrete pole equations for $c \rightarrow 1^-$ supports the first conjecture, and the results of Sec. III-IV will confirm and quantify both.

To this end, another method is devised to compute the flame shapes analytically. The key step is to introduce an appropriate *resolvent*, which can be interpreted as a complex electric (or velocity) field caused by charges (or fluid sources) distributed according to the unknown pole density profile. The equations that rule the positions of the poles then turn into a nonlocal, scalar Riemann-Hilbert problem for the resolvent, which might be solved by complex analysis techniques. The advantage of this method is that, once the resolvent is found, the pole density and the front slope can be obtained easily, without extra integration.

In this way, we reproduce the results obtained in [20] for $-1 \leq c \leq 0$, and explain and fix the pathologies of (3) for $c > 0$. The method is valid whatever the sign of c , and generalizes results on wrinkled fronts with two unlike crests per wavelength, which was so far available for the MS equation only [19]. In all the configurations envisaged, we compare the analytical predictions with numerical determinations of the discrete B_k and of ϕ .

The paper is organized as follows. In Sec. II, the pole decompositions and their continuous approximations are introduced. We introduce at a formal level the notion of resolvent and we give equivalent forms of the ZT equation in § II C. The resolvent approach is then exploited for isolated crests (Sec. III), and next adapted to two-crested x -periodic fronts (Sec. IV); in both cases comparisons with numerical results are presented and discussed. We summarize our results and formulate open problems concerning flame shapes in Section V. A resolution of the discrete pole equations for $c \rightarrow 1^-$, and technical details about resolvent determinations, are presented in Appendices A and B respectively.

We also find links between flames fronts governed by the ZT equation, and other statistical-mechanical problems inspired from random matrix theory. Since the main body of the article is devoted to flames, we postpone this discussion to Appendix C.

II. POLE DECOMPOSITIONS, ISOLATED CRESTS AND THE LIMIT OF LARGE CRESTS

A. Discrete poles

Once properly shifted as to be centered, steady isolated crests of infinite wavelengths have $\phi = \phi(x)$ where ϕ_x is a sum of $2N$ simple pole contributions $\propto \frac{1}{x-iB_k}$, $|k| = 1, \dots, N$. $B_{-k} = -B_k$ ensures that $\phi(x)$ is real valued when x is real. Since $\mathcal{H}[\frac{1}{x-iB}] = \frac{-i\text{sgn}(B)}{x-iB}$, the dominant balance in (1) implies that each pole has residue $\frac{-2\nu}{1-c}$:

$$\phi_x = \frac{-2\nu}{1-c} \sum_{\substack{k=-N \\ k \neq 0}}^N \frac{1}{x-iB_k}. \quad (4)$$

For (1) to be satisfied, the pole altitudes B_k obey coupled equations, originally expressed for $k = \pm 1, \dots, \pm N$ as [18]:

$$\sum_{\substack{j=-N \\ j \neq 0, k}}^N \frac{1-c \text{sgn}(B_k) \text{sgn}(B_j)}{(1-c)(B_k - B_j)} = \frac{\text{sgn}(B_k)}{2\nu}. \quad (5)$$

Without loss of information, (5) may be rewritten in terms of $B_1, \dots, B_N > 0$ only. For $k = 1, \dots, N$:

$$\sum_{\substack{j=1 \\ j \neq k}}^N \frac{1}{B_k - B_j} + \frac{1+c}{1-c} \sum_{j=1}^N \frac{1}{B_k + B_j} = \frac{1}{2\nu}, \quad (6)$$

whereby the discontinuous $\text{sgn}(B)$ function no longer shows up.

Summing B_k (Eq. (6)) yields $0 < B_1 + \dots + B_N = \nu N (\frac{2N}{1-c} - 1)$, whence $c < 1$. This must be considered jointly with the constraint $-1 \leq c$ needed from $B_1/\nu > 0$ (obtained for $c \rightarrow -1$, cf. [20]). For any fixed $-1 \leq c < 1$, the B_k 's will scale like νN if $N \rightarrow \infty$, as in the $c = 0$ case, whereby the typical spacing $B_k - B_{k-1}$ is $\sim \nu \sim B_N/N$. One may thus introduce a density

$$\varrho(B) \geq 0 \quad (7)$$

here such that $\varrho(B)dB$ measures the number of poles with *positive* altitudes in $[B, B + dB]$. This continuous approximation enables to rewrite (6) as an integral equation, valid for $B \in [B_{\min}, B_{\max}]$:

$$\oint_{B_{\min}}^{B_{\max}} \frac{\varrho(B') dB'}{B - B'} - \frac{\mathbf{n}}{2} \int_{B_{\min}}^{B_{\max}} \frac{\varrho(B') dB'}{B + B'} = \frac{1}{2\nu}, \quad (8)$$

where \oint denotes the Cauchy principal value, and the constant \mathbf{n} is defined as:

$$\mathbf{n} = -2 \frac{1+c}{1-c}. \quad (9)$$

Notice that $-1 < c < 0$ is mapped to $-2 < \mathbf{n} < 0$, and it will be convenient to set in this regime $c = -\tan^2(\pi\gamma/2)$, so that:

$$0 < \gamma < 1/2, \quad \mathbf{n} = -2 \cos(\pi\gamma). \quad (10)$$

When $0 < c < 1$, we rather have $\mathbf{n} < -2$, and a convenient parametrization is $c = \tanh^2(\pi\gamma/2)$, so that:

$$0 < \gamma, \quad \mathbf{n} = -2 \cosh(\pi\gamma). \quad (11)$$

The equation (8) must be solved subjected to the normalization condition:

$$\int_{B_{\min}}^{B_{\max}} \varrho(B) dB = N, \quad (12)$$

and the continuous version of (4) will express the front slope ϕ_x in terms of $\varrho(B)$ as:

$$\phi_x(x) = \frac{4\nu}{1-c} \text{Im} \left(\int_{B_{\min}}^{B_{\max}} \frac{\varrho(B) dB}{ix - B} \right). \quad (13)$$

The above $\varrho(B)$ may be nonzero for $B \geq 0$ *only*, contrary to the two-sided even density $\rho(B) = \varrho(B) + \varrho(-B)$ employed in [20]. Also notice that (8) allows for a lower end $B_{\min} \geq 0$ of the density support, besides the upper end B_{\max} ; both have to be determined as parts of the solution. For $c \leq 0$, B_{\min} happened to vanish [20], whereas an argument presented in Appendix A shows that $B_{\min} > 0$ in the limit $c \rightarrow 1^-$. One of the outcome of this article is that $B_{\min} > 0$ for any $0 < c < 1$ (see Fig. 1), while $B_{\min} = 0$ for any $-1 < c \leq 0$.

B. Preliminary comments

The kind of systems (5), which express a repulsion between the poles B_k and some of their images (here the $B_{-k} = -B_k$) with possibly different intensity (here, if $k, k' \geq 1$, the interaction of B_k and $B_{-k'}$ is $(-\mathbf{n}/2)$ times stronger than the mutual interaction between B_k and $B_{k'}$), is ubiquitous in statistical physics. In the context of quantum integrable system, they typically appear as the result of a *Bethe Ansatz* to determine the eigenvalues of transfer matrices. This repulsion phenomenon is also observed for the zeros of orthogonal polynomials [22], optimal approximation points and the eigenvalues of random matrices [23, 24]. The connection between those topics and flame fronts is not accidental: we point out in Appendix C that the ZT equation coincides with the large N limit of a Schwinger-Dyson equation in a statistic-mechanical ensemble of N particles called "β-deformed $\mathcal{O}(\mathbf{n})$ matrix model".

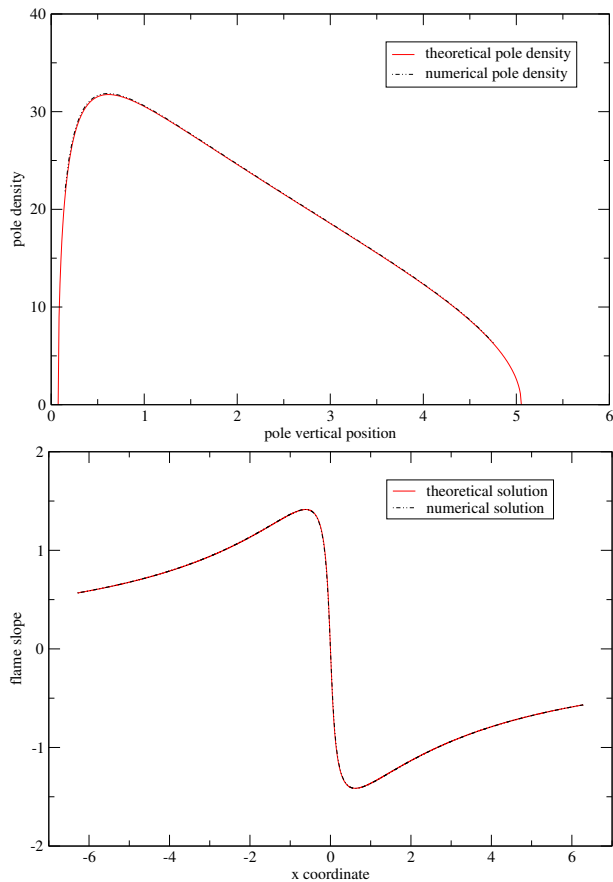


FIG. 1. Comparison of theoretical and numerical pole density (top, theoretically given by (44)) and flame slope (bottom, theoretically given by (47)) for an isolated crest with $c > 0$. The plot assumes $c = 0.5$, $N = 100$ and $1/\nu = 199.5$.

The problem of describing how poles satisfying an equation like (5) condense when N is large, i.e. of solving singular integral equations like (8), is sometimes more convenient to consider from the point of view of complex analysis. There often exists an appropriate Riemann surface containing the support of ϱ , on which the density can be continued to an analytic function $\tilde{\varrho}$. One can then use the powerful tools of algebraic geometry to determine it, in particular the behavior of $\tilde{\varrho}$ at its singularities fixes much of the solution. We may bring up in the same spirit the techniques of conformal mapping used to solve Dirichlet problems for harmonic functions, which is well-known in electrostatics. The techniques to solve (8) effectively have been developed prior to this work in the context of matrix models, for all values of c [25–28]. In this article, we adapt them to the determination of flame shapes.

Before going into details, it is noteworthy that the behavior of ϱ at the edges of the supports features some universality: it depends only on the type of short-distance repulsion between poles, and does not on the details of external potential (the right-hand side in (8)). If B_k remains away from their images, the density will typically behave as a squareroot near $B_{\min} > 0$. With (8) this hap-

pens for $c > 0$, and obviously the flame slope $\phi_x(x)$ will be smooth near $x = 0$. But if $B_{\min} = 0$, the poles close to 0 are subjected to a strong self-interaction but also a strong interaction with their images at opposite position since the latter are also close to 0. The exponent α such that $\varrho(B) \propto B^{-\alpha}$ when $B \rightarrow 0^+$ now depends continuously on the relative strength of interactions (see Sec III B)

$$\alpha = \gamma = \frac{1}{\pi} \cos^{-1}(-n/2) = \frac{2}{\pi} \tan^{-1}(\sqrt{-c}) \quad (14)$$

With (8), this results for $-1 < c \leq 0$ in a cusp of the flame profile at $x = 0$, such that $\phi_x(x) \propto -\text{sgn}(x)|x|^{-\gamma}$.

Anticipating on Sec. III, we find that the exact solution of (8) nicely agrees with what the numerical resolution of the discrete pole equations (6) gives for $N \gg 1$, and with the slope $\phi_x(x)$ ensuing from (13). In the regime $-1 < c \leq 0$, this exact solution is constructed in § III C and was already known and compared to numerics in [20, Fig. 3]; the corresponding flame profile has a cusp as we just discussed. For $0 < c < 1$, the exact solution is devised in § III B and displayed in Fig. 1. Unlike [20, Fig. 5] where the pathological formula (3) was plotted, the theoretical prediction in Fig. 1 does not feature a singularity at $x = 0$, as it should be (we used in both plots the exact same parameters).

C. Continuum of poles and resolvents

A function $\phi_x(x)$ (assumed square-integrable) can always be represented uniquely as [29]:

$$\phi_x(x) = \frac{4\nu}{1-c} \text{Im } W(ix) \quad (15)$$

where $W(z)$ is a holomorphic function in the domain $\{\text{Re } z < 0\}$, called *resolvent*. In this paragraph – which can be read independently – we clarify what does it mean for $\phi_x(x)$ to solve the ZT equation in terms of the resolvent, and therefore put the discrete pole decompositions (4) in a broader perspective. A more elementary approach will be adopted in § III A.

Let us look for solutions of ZT such that $W(z)$ is actually holomorphic in $\mathbb{C} \setminus \mathcal{C}$, where \mathcal{C} is a reunion of bounded arcs in the region $\{\text{Re } z \geq 0\}$, which is invariant by complex conjugation. We allow \mathcal{C} to touch finitely many times the axis $i\mathbb{R}$: these points of contact would correspond to singularities of $\phi_x(x)$. Besides, we assume that the front is asymptotically flat, i.e. $W(z) = o(1)$ when $z \rightarrow \infty$. Then, we can use Cauchy residue formula to represent:

$$W(z) = \int_{\mathcal{C}} \frac{\varrho(B) dB}{z - B} \quad (16)$$

where we introduced the density:

$$\varrho(B) = \frac{W(B - i0) - W(B + i0)}{2i\pi} \quad (17)$$

The discrete pole decomposition (4) corresponds to the special case where $\varrho(B)$ is a sum of N Dirac masses located at $B = B_k$ for $k = 1, \dots, N$. Here, we rather want to consider the case where $\varrho(B)$ is continuous.

The assumption $\mathcal{C} = \mathcal{C}^*$ allows to rewrite (15) as:

$$\phi_x(x) = \frac{2\nu}{i(1-c)} [W(ix) - W(-ix)], \quad (18)$$

when $x \in \mathbb{R}$ is not at a singularity of $\phi_x(x)$. Thanks to the assumed analytic properties of $W(z)$, the Hilbert transform of $\phi_x(x)$ can be computed explicitly:

$$\mathcal{H}[\phi_x](x) = \frac{2\nu}{1-c} [W(ix) + W(-ix)]. \quad (19)$$

Therefore, the ZT equation is equivalent to: for any $z \in i\mathbb{R}$,

$$\begin{aligned} W^2(z) + W^2(-z) + \mathbf{n}W(z)W(-z) \\ + W'(z) + W'(-z) - (1/\nu)[W(z) + W(-z)] = 0. \end{aligned} \quad (20)$$

where \mathbf{n} was defined in (9). And, since (20) is an equality between analytic functions, it must be valid in the whole domain of analyticity, namely for any $z \in \mathbb{C} \setminus \mathcal{C}$.

Large wrinkles correspond to the limit $\nu \rightarrow 0$ but with $W(z)$ scaling like $1/\nu$ so as to keep a macroscopic front slope in (15). In this limit, the derivative term in (20) can be neglected and we find $\mathcal{E}[W](z) = 0$, where we set:

$$\begin{aligned} \mathcal{E}[W](z) = W^2(z) + W^2(-z) + \mathbf{n}W(z)W(-z) \\ - (1/\nu)[W(z) + W(-z)]. \end{aligned} \quad (21)$$

Computing the discontinuity of $\mathcal{E}[W](z)$ at a point $B \in \mathcal{C}$, we find:

$$\begin{aligned} [W(B+i0) - W(B-i0)] \\ \times [W(B+i0) + W(B-i0) + \mathbf{n}W(-B) - 1/\nu] = 0. \end{aligned} \quad (22)$$

Therefore:

$$W(B+i0) + W(B-i0) + \mathbf{n}W(-B) = 1/\nu. \quad (23)$$

In terms of the density $\varrho(B)$, this equation is equivalent to (8) which has been derived in § II A for the continuum limit of a discrete pole configuration.

Conversely, imagine that we have a function $W(z)$ is holomorphic in a domain $\mathbb{C} \setminus \mathcal{C}$, which decays at infinity, which has a continuous density $\varrho(B)$, and which satisfies (23). It follows that $\mathcal{E}[W](z)$ is holomorphic on $\mathbb{C} \setminus (\mathcal{C} \cup -\mathcal{C})$ and decays at infinity. Furthermore, by multiplying (23) by $W(B+i0) - W(B-i0)$ and rearranging, we find that $\mathcal{E}[W](z)$ is continuous across \mathcal{C} . By parity, it is also continuous across $-\mathcal{C}$, and therefore, $\mathcal{E}[W](z)$ is an entire function decaying at infinity. By Liouville theorem, it must vanish: in other words, $\phi_x(x)$ given by (15) is solution to the ZT equation (1) in the limit of large wrinkles.

III. RESOLVENTS AND ISOLATED CRESTS

A. Strategy

Even without referring to § II C, the form of (8) suggests to introduce the so-called resolvent, defined for a complex variable z as:

$$W(z) = \int_{B_{\min}}^{B_{\max}} \frac{\varrho(B) dB}{z - B}. \quad (24)$$

In the context of an electrostatic (of a fluid-mechanical) analogy, $W(z)$ would represent the complex electric (or velocity) field generated by charges (or fluid sources) deposited according to the density $\varrho(B)$ along the segment $[B_{\min}, B_{\max}]$ in the z -complex plane. Equivalently, $W(z)$ is the unique function which is holomorphic on $\mathbb{C} \setminus [B_{\min}, B_{\max}]$, behaves as N/z when $z \rightarrow \infty$, and is discontinuous on $[B_{\min}, B_{\max}]$ with a given jump:

$$\frac{W(B-i0) - W(B+i0)}{2i\pi} = \varrho(B). \quad (25)$$

The Cauchy principal value in (8) can then be expressed as:

$$\oint_{B_{\min}}^{B_{\max}} \frac{\varrho(B') dB'}{B - B'} = \frac{W(B-i0) + W(B+i0)}{2}. \quad (26)$$

We can also reformulate (8) in terms of the resolvent only: for $B \in [B_{\min}, B_{\max}]$,

$$W(B+i0) + W(B-i0) + \mathbf{n}W(-B) = 1/\nu. \quad (27)$$

The normalization condition (12) is translated into the requirement:

$$W(z) \sim N/z, \quad z \rightarrow \infty, \quad (28)$$

and the front slope can be expressed readily by comparing of (13) and (24):

$$\phi_x(x) = \frac{4\nu}{1-c} \text{Im}[W(ix)]. \quad (29)$$

The strategy to solve (27) has been developed in [27, 28]. The first step is to assume that the position of the density support $[B_{\min}, B_{\max}]$ is given, and determine it by consistency only at the end. The second step consists in performing a change of variable which uniformizes the complex plane with two cuts $[B_{\min}, B_{\max}]$ and $[-B_{\max}, -B_{\min}]$, since points on these two segments are involved in (27). In other words, one constructs:

$$\omega(\psi) = W(z(\psi)), \quad (30)$$

where ψ belongs to some domain \mathcal{D} in the complex plane, so that (27) relates boundary values of ω on \mathcal{D} , in such a way that its resolution becomes "easy" using Schwarz reflection principle. This can be done with trigonometric functions if $B_{\min} = 0$, whereas elliptic functions shows up

if $B_{\min} > 0$. The third step is the resolution of the equation for ω taking into account its analytical properties and the normalization (12), which result in the determination of the position of the support $[B_{\min}, B_{\max}]$. If several solutions for the support are available, there is in general a unique one which ensures positivity of the density (7). We already announce the result that $B_{\min} = 0$ whenever $-1 < c < 0$, while $B_{\min} > 0$ in the case $0 < c < 1$, and we now explain the implementation of this method in both cases. The limit cases $c = -1, 0, 1$ are better discussed separately, respectively in [20], [19] and Appendix A.

B. Solution for $0 < c < 1$

We assume in this paragraph $B_{\min} > 0$, and later find this implies $0 < c < 1$. It is convenient to choose as change of variable:

$$z = B_{\min} \operatorname{sn}_k(\psi), \quad k = \frac{B_{\min}}{B_{\max}}, \quad (31)$$

where sn is the Jacobi elliptic sine function [30]. Let K and K' be the complete elliptic integrals with modulus k . The z -complex plane with its two cuts $[-B_{\max}, -B_{\min}] \cup [B_{\min}, B_{\max}]$ is mapped onto the rectangle \mathcal{D} of vertices $\pm K$ and $\pm iK'$ (see Fig. 2). More precisely: the segment $[B_{\min}, B_{\max}] \pm i0$ is mapped to the half-edge $[K, K \pm iK']$ in the rectangle; the lower (resp. upper) side of the segment $] -\infty, -B_{\max}] \cup [B_{\max}, +\infty[$ is mapped to the upper (resp. lower) horizontal edge of the rectangle, and in particular the point $z = \infty$ correspond to $\psi = \pm iK'$; and the segment $] -B_{\max}, -B_{\min}] \pm i0$ is mapped to $[-K, -K \pm iK']$.

$\omega(\psi) = W(z(\psi))$ defines a holomorphic function in the rectangle \mathcal{D} . The analytical properties of the resolvent (24) provide relations between values of ω on the boundary of \mathcal{D} . Firstly, since the resolvent is continuous across $] -\infty, -B_{\max}] \cup [B_{\max}, +\infty[$, we must have:

$$\omega(\psi) = \omega(\psi + 2iK'), \quad (32)$$

when ψ belongs to the lower horizontal edges of \mathcal{D} . Similarly, the continuity of $W(z)$ across $[-B_{\max}, -B_{\min}]$ implies:

$$\omega(\psi) = \omega(-2K - \psi), \quad (33)$$

when ψ belongs to the edge $[-K - iK', -K + iK']$. Eventually, (27) itself is equivalent to:

$$\omega(\psi) + \omega(\psi - 4K) + \mathbf{n}\omega(\psi - 2K) = 1/\nu, \quad (34)$$

when ψ belongs to the edge $[K - iK', K + iK']$.

The key observation is that successive applications of Schwarz reflection principle and (32)-(34) allows to continue analytically ω on the whole ψ -complex plane, so that (32)-(34) are satisfied *everywhere*. Indeed, (32) allows to define $\omega(\psi)$ as a $2iK'$ -periodic function on the strip $\mathcal{S} = \{-K < \operatorname{Re} \psi < K\}$, while (33) allows to define

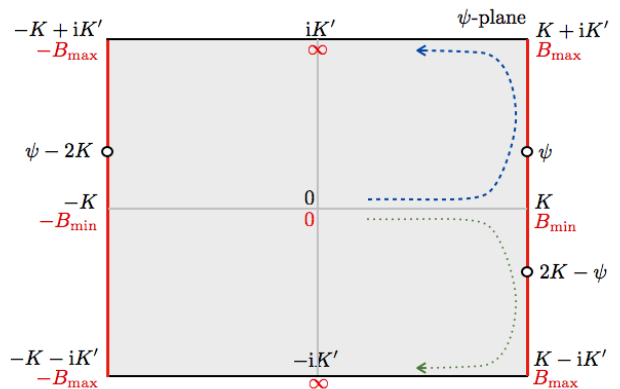
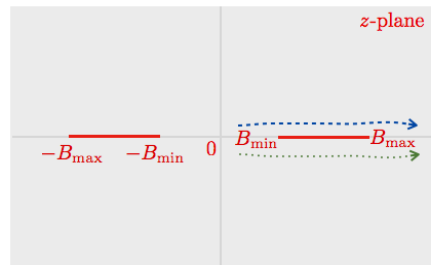


FIG. 2. Mapping between the z -plane (top panel) with its two cuts on $[-B_{\min}, -B_{\max}] \cup [B_{\min}, B_{\max}]$ and the rectangle \mathcal{D} in the ψ -plane (lower panel). For special points in the ψ -plane, we indicate below (in red) the corresponding value of z . The dashed blue and dotted green paths indicates how the mapping "opens" the cuts.

$\omega(\psi)$ on the doubled strip $\mathcal{S}_2 = \{-3K < \operatorname{Re} \psi < K\}$. Then, (34) provides a relation between values of ω on the boundary of \mathcal{S} . Furthermore, if we take a point $\psi \in \mathcal{S}_2 - 4K$, the points $\psi - 2K$ and ψ belong to \mathcal{S}_2 . So, enforcing (34) defines $\omega(\psi)$ as an analytic function of $\psi \in \mathcal{S}'_2 = \mathcal{S}_2 \cup (\mathcal{S}_2 - 4K)$, which satisfies (34) everywhere on \mathcal{S}'_2 . This argument can be used recursively to analytically continue $\omega(\psi)$ on all strips of the form $\mathcal{S}_2 + 4mK$ for any integer m , so as to cover the whole complex plane.

The problem is now reduced to an easier one, namely finding the most general analytic functions which satisfy (32)-(34), i.e. with an appropriate behavior under $2K$ and $2iK'$ translations of their argument. The general solution can be put in the form:

$$\omega(\psi) = \frac{1}{\nu(2 + \mathbf{n})} + g(\psi)\omega_+(\psi) + g(-\psi)\omega_+(-\psi - 2K), \quad (35)$$

where $g(\psi)$ is an arbitrary analytic function which is $2K$ and $2iK'$ periodic, and $\omega_+(\psi)$ is any analytic function satisfying:

$$\omega_+(\psi + 2iK') = \omega_+(\psi), \quad \omega_+(\psi + 2K) = e^{\pi\gamma}\omega_+(\psi), \quad (36)$$

Here, the parametrization (11) $\mathbf{n} = -(e^{\pi\gamma} + e^{-\pi\gamma})$ arises quite naturally. In (35), the constant term is an obvious

particular solution of the inhomogeneous equation (34), while the second term is the general solution of (32)-(34) with vanishing right-hand side.

Notice that, since W was holomorphic on $\mathbb{C} \cup \{\infty\} \setminus [B_{\min}, B_{\max}]$, and the right-hand side of (34) is a constant, $\omega(\psi)$ must be an entire function. Therefore, in the solution we are looking for, $g(\psi)\omega_+(\psi)$ (which also satisfies (36)) is entire as well. We explain in Appendix B that this is impossible, unless:

$$\gamma K' = 2pK \quad \text{for some positive integer } p. \quad (37)$$

In particular, γ must be real, hence $c > 0$. Besides, when (37) holds, we easily guess a holomorphic solution of (36):

$$\omega_+(\psi) = e^{\pi p \psi / K'}. \quad (38)$$

With this choice, we are looking for an entire function $g(\psi)$ which is biperiodic, hence bounded, hence constant by Liouville theorem. We thus obtain

$$\omega(\psi) = \frac{1}{\nu(2+n)} + G \cosh[\pi(\gamma/2 + \psi/K')], \quad (39)$$

for some constant G . The normalization (28) implies two consistency equations given by:

$$\omega(\psi) \Big|_{\psi \rightarrow iK'} = 0 + \frac{N}{B_{\max}}(\psi - iK') + o(\psi - iK'). \quad (40)$$

Jointly with (37), they provide three equations for the three unknowns B_{\min} , B_{\max} and G . The integer p seems to allow for a discrete set of solutions, but we now argue that $p = 1$ is the only one which is physically admissible. Indeed, let us come back to the density of poles (25). After our change of variables, it can be expressed as:

$$\varrho(B) = \frac{\omega(K - i\chi(B)K') - \omega(K + i\chi(B)K')}{2i\pi} \quad (41)$$

where $0 < \chi(B) < 1$ is the unique point for which $\psi(B) = K + i\chi(B)K'$ satisfies (31) for $z = B$. Inserting (39) into (41), we find:

$$\varrho(B) = -\frac{4G}{\pi} \frac{\sqrt{c}}{1-c} \sin[\pi p \chi(B)] \quad (42)$$

Since the sign of $\varrho(B)$ is not allowed to change on the support, we must impose $p = 1$.

The final answer for the resolvent can be written:

$$W(z(\psi)) = -\frac{1}{4\nu} \frac{(1-c)^{3/2}}{c} \times \left\{ \frac{1}{\sqrt{1-c}} + \cosh[\pi(\gamma/2 + \psi/K')] \right\}, \quad (43)$$

and the corresponding pole density is:

$$\varrho(B) = \frac{1}{2\pi} \sqrt{\frac{1-c}{c}} \frac{1}{\nu} \sin[\pi \chi(B)]. \quad (44)$$

We can give an alternative definition for the function $\chi(B)$ in terms of Jacobi elliptic functions [30]: if we set $k' = \sqrt{1-k^2}$,

$$\chi(B) = \frac{1}{K'} \text{nd}_{k'}^{-1} \left(\frac{B}{B_{\min}} \right). \quad (45)$$

The ratio $k = B_{\min}/B_{\max}$ is fixed as a function of $c = \tanh^2(\pi\gamma/2)$ by (37) with $p = 1$, and then we find from (40)

$$B_{\max} = \frac{8K}{\pi\gamma} \frac{\sqrt{c}}{1-c} \nu N. \quad (46)$$

To conclude, formula (29) delivers the expression of the front slope:

$$\phi_x(x) = -\frac{1}{\sqrt{c}} \sin \left[\frac{\pi}{K'} \text{sc}_{k'}^{-1} \left(\frac{x}{B_{\min}} \right) \right], \quad (47)$$

where $\text{sc}_{k'}^{-1}$ is the reciprocal function of the Jacobi elliptic function $\text{sc}_{k'} = \text{sn}_{k'}/\text{cn}_{k'}$. These results are in agreement with the numerical resolution of (6), see Fig. 1.

C. Solution for $-1 < c < 0$

As we explained, the only possibility in this case is $B_{\min} = 0$. It corresponds to the limit $k \rightarrow 0$, and thus $K \rightarrow \pi/2$ in the former construction, in which the Jacobi elliptic function degenerates to trigonometric functions. We prefer to use the change of variable:

$$z = \frac{B_{\max}}{\cosh \psi}. \quad (48)$$

which, although not exactly the limit of (31), is closely related. Thanks to (48), the z -complex plane with its two cuts $[-B_{\max}, 0] \cup [0, B_{\max}]$ is mapped onto the strip $\mathcal{D} = \{0 < \text{Im } \psi < \pi\}$ (see Fig. 3). More precisely, the segment $[0, B_{\max}] \pm i0$ is mapped to the half-line \mathbb{R}_{\mp} ; the segment $[-B_{\max}, 0] \pm i0$ is mapped to the half-line $i\pi + \mathbb{R}_{\mp}$; the point $z = \infty$ is mapped to $\psi = i\pi/2$.

$\omega(\psi) = W(z(\psi))$ defines a holomorphic function on the strip \mathcal{D} . Since the analysis now parallels the case $c > 0$, we go quickly over it. Continuity of the resolvent $W(z)$ across $[-B_{\max}, 0]$ implies

$$\omega(\psi) = \omega(2i\pi - \psi) \quad (49)$$

when $\text{Im } \psi = \pi$, and (27) translates into

$$\omega(\psi) + \omega(-\psi) + n\omega(\psi + i\pi) = 1/\nu \quad (50)$$

when ψ belongs to \mathbb{R} . These relations can be used to analytically continue $\omega(\psi)$ in the whole complex plane, so that (49)-(50) are satisfied everywhere, or equivalently (49) and

$$\omega(\psi) + \omega(\psi + 2i\pi) + n\omega(\psi + i\pi) = 1/\nu. \quad (51)$$

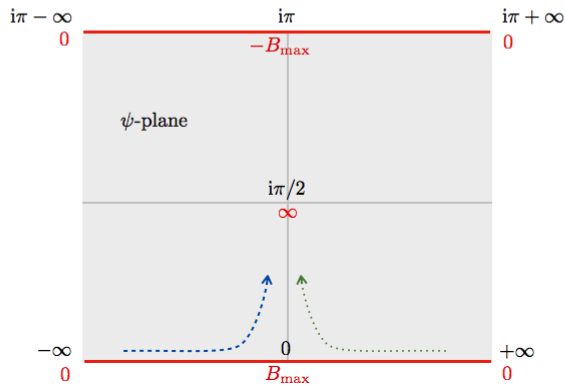


FIG. 3. Mapping between the z -plane with two merged cuts $[-B_{\max}, 0] \cup [0, B_{\max}]$ and the strip \mathcal{D} in the ψ -plane (values in black). For special points in the ψ -plane, we indicate below (in red) the corresponding value of z . The blue dashed (resp. green dotted) arrow indicates the image in the ψ -plane of a path in the z -plane with positive (resp. negative) imaginary part.

The general solution of (49)-(50) can be written:

$$\omega(\psi) = \frac{1}{\nu(2+\mathbf{n})} + g(\psi)\omega_+(\psi) + g(-\psi)\omega_+(2i\pi - \psi), \quad (52)$$

where $g(\psi)$ is an arbitrary $i\pi$ periodic, analytic function, and ω_+ is any analytic function satisfying:

$$\omega_+(\psi + i\pi) = e^{i\pi\gamma}\omega_+(\psi). \quad (53)$$

where we recall the parametrization (10) $\mathbf{n} = -(e^{i\pi\gamma} + e^{-i\pi\gamma})$. A possible choice is:

$$\omega_+(\psi) = \frac{e^{(\gamma-1)\psi}}{\sinh(\psi)}. \quad (54)$$

Our change of variable (48) sends the point $z = 0$ at $\psi = \pm\infty$, and more precisely $z \sim (B_{\max}/2)e^{\mp\psi}$. So, we have to be careful that $W(\psi)$ does not grow too much when $\psi \rightarrow \pm\infty$ so that the pole density $\varrho(B)$ remains integrable at $B = 0$. This condition is equivalent to demanding that $W(\psi)$ be $o(e^\psi)$ when $\psi \rightarrow +\infty$. Being a $i\pi$ periodic function, $g(\psi)$ admits a Fourier expansion $g(\psi) = \sum_{p \in \mathbb{Z}} \hat{g}_p e^{2p\psi}$. The integrability condition results in $\hat{g}_p = 0$ whenever $p \neq 0, 1$. Besides, since the right-hand side of (50) is a constant, we find that $\omega(\psi)$ is an entire function. We deduce that, in the solution we are looking for, $g(\psi)$ must be holomorphic, and such that the apparent pole of (54) at $\psi = i\pi$ is absent in (52). This gives a relation between \hat{g}_0 and \hat{g}_1 , and leads eventually to our solution in the form:

$$\omega(\psi) = \frac{1}{\nu(2+\mathbf{n})} + G \cosh[\gamma(\psi - i\pi)] \quad (55)$$

for some constant G . The normalization condition (28)

becomes:

$$\omega(\psi)_{\psi \rightarrow i\pi/2} = 0 + \frac{iN}{B_{\max}}(\psi - i\pi/2) + o(\psi - i\pi/2), \quad (56)$$

and provides two equations determining the two unknowns B_{\max} and G . We find that the maximal position of the poles is:

$$B_{\max} = \frac{4}{\gamma} \frac{\sqrt{-c}}{1-c} N\nu. \quad (57)$$

We thus find a unique solution for the resolvent:

$$W(z(\psi)) = \frac{1}{4\nu} \frac{(1-c)^{3/2}}{-c} \left(\frac{1}{\sqrt{1-c}} - \cosh[\gamma(\psi - i\pi)] \right), \quad (58)$$

and as expected, the corresponding pole density is positive:

$$\varrho(B) = \frac{1}{2\pi} \sqrt{\frac{1-c}{-c}} \frac{1}{\nu} \sinh \left[\gamma \cosh^{-1} \left(\frac{B_{\max}}{B} \right) \right], \quad (59)$$

The flame slope is retrieved from (29):

$$\phi_x(x) = -\frac{1}{\sqrt{-c}} \sinh \left[\gamma \sinh^{-1} \left(\frac{B_{\max}}{x} \right) \right]. \quad (60)$$

We observe a strong similarity with the results of the regime $0 < c < 1$, namely (43)-(47). Going from $c > 0$ to $c < 0$, one just need to replace c by $-c$, the elliptic functions by their trigonometric analog, and γ is replaced by $i\gamma$, so that trigonometric functions rather appears as hyperbolic functions.

D. Discussion

The first noteworthy point concerns $-1 < c < 0$: the results (57) and (59)-(60) then coincide with those found in [20], up to slightly different notations (e.g., γ was called μ whereby $\frac{2\sqrt{-c}}{\gamma(1-c)} = \frac{\sin \pi\mu}{\mu}$) and thanks to such identities as $2 \sinh^{-1} \left(\frac{1}{\sinh \xi} \right) = \text{sgn}(\xi) \ln \left(\frac{1}{\tanh^2(\xi/2)} \right)$.

If $0 < c < 1$, however, the above exact results do differ from those found in [20] by naive continuation from $c < 0$. In particular, (47) and (44)-(45) are free of the oscillations that crippled (3) and the corresponding density profile. To explain why the latter "solutions" were nevertheless so close to their numerical counterpart over the $x + iB = O(N\nu)$ range when $0 \leq c \lesssim 0.6$, one first notices that the maximum pole altitude B_{\max} in (46) and the quantity $B_* = \frac{4}{\gamma} \frac{\sqrt{c}}{(1-c)} \nu N$ featured in (3) are related by

$$\frac{B_{\max}}{B_*} = \frac{2K}{\pi} \underset{k \rightarrow 0}{=} 1 + O(k^2) \quad (61)$$

As $K' = \ln(4/k) + o(1)$ when $k \rightarrow 0$, $\gamma \sim \frac{2\sqrt{c}}{\pi}$ must be small in (37) for $p = 1$, which implies:

$$k \sim 4 \exp \left(-\frac{\pi^2}{2\sqrt{c}} \right) \quad (62)$$

The ratio $k = \frac{B_{\min}}{B_{\max}}$ is thus exceedingly small if $0 < c \ll 1$, and it remains small if $0 \leq c \lesssim 0.6$ thanks to the π^2 constant in (62): B_* and B_{\max} are then nearly equal. Similarly, the difference between (47) and (3) is strongly suppressed by $O(k^2)$ factors wherever $|x| \gg B_{\min}$; this is enough for (3) to accurately capture the crest slope profile, the exact maximum $\max |\phi_x(x)| = c^{-1/2}$ (reached at $|x|/B_{\min} \sim k^{-1/2} \gg 1$) inclusive.

The discarded unphysical profiles associated with integers $p > 1$ in (37) would have had an extra p in the exponent of (62). And, as $p \rightarrow \infty$ at fixed $0 < c < 1$ in (37) leads to $k \rightarrow 0$ and $B_{\min} \rightarrow 0$, the front slope $\phi_x(x)$ given by (47) would resume (3). Indeed, the only "error" in (3) was the implicit assumption that $B_{\min}/B_{\max} = 0$, as when $c < 0$.

Next, for $k \rightarrow 1^-$, we have $K' \sim \pi/2$ and $K = \frac{1}{2} \ln\left(\frac{8}{(1-k)}\right) + o(1)$, while $\pi\gamma = \ln\left(\frac{4}{1-c}\right) + o(1)$ if $c \rightarrow 1^-$; equations (37) and (46) then reduce to:

$$\left(1 - \frac{B_{\min}}{B_{\max}}\right) \sim 4\sqrt{1-c}, \quad B_{\max} \sim \frac{2\nu N}{1-c} \quad (63)$$

quite in line with Appendix A. Using the integral representation of nd_k^{-1} [31, p. 494] in (44)-(45) and (62), one can show that (44) resumes the Marčenko-Pastur law when $c \rightarrow 1^-$.

IV. BICOALESCED PERIODIC FRONTS

A. Integral equations for pole densities

We now consider steady periodic cells, for which $\phi(t, x) = -Vt + \phi(x)$; the drift velocity was calculated in [18] in terms of the neutral-to-actual wavelength $\nu \in]0, 1[$ and the total number N of pairs of poles involved $V = \frac{2N\nu(1-N\nu)}{1-c}$. Upon rescaling of the space coordinate, we may assume that $\phi_x(x)$ is 2π -periodic. We will address more specifically the issue of bicoalesced periodic fronts. These are obtained as periodic solutions of the ZT equation which admit a pole decomposition, with two vertical piles of poles separated by a half-wavelength:

$$\phi_x(x) = \sum_{\substack{k=-N_1 \\ k \neq 0}}^{N_1} \frac{-\frac{\nu}{1-c}}{\tan\left(\frac{x-iB_k}{2}\right)} + \sum_{\substack{m=-N_2 \\ m \neq 0}}^{N_2} \frac{-\frac{\nu}{1-c}}{\tan\left(\frac{x-\pi-ib_m}{2}\right)} \quad (64)$$

A large number of these bicoalesced solutions have been obtained in [32] in the Michelson-Sivashinsky case $c = 0$, all of which have been found to be stable with Neumann boundary conditions in the same paper. A solution of this type, obtained by direct numerical simulation, is presented in [33]. Periodic configurations featuring a single pile of pole can be extracted from (64) by assuming $N_2 = 0$, or assuming $N_1 = N_2$ and $b_k = B_k$, and doubling the wavelength. The analysis of such solutions is parallel to that of isolated crests. Plugging (64) in the ZT equation fixes the prefactor equal to $\frac{-\nu}{1-c}$, and yields

coupled equations for the position of the poles. In the first pile, we have for any $k = 1, \dots, N_1$,

$$\sum_{\substack{j=1 \\ j \neq k}}^{N_1} \frac{1}{\tanh\left(\frac{B_k - B_j}{2}\right)} - \frac{\mathfrak{n}}{2} \sum_{j=1}^{N_1} \frac{1}{\tanh\left(\frac{B_k + B_j}{2}\right)} \quad (65)$$

$$+ \sum_{m=1}^{N_2} \tanh\left(\frac{B_k - b_m}{2}\right) - \frac{\mathfrak{n}}{2} \sum_{m=1}^{N_2} \tanh\left(\frac{B_k + b_m}{2}\right) = f,$$

and symmetrically in the second pile, we have for any $m = 1, \dots, N_2$:

$$\sum_{\substack{l=1 \\ l \neq m}}^{N_2} \frac{1}{\tanh\left(\frac{b_m - b_l}{2}\right)} - \frac{\mathfrak{n}}{2} \sum_{l=1}^{N_2} \frac{1}{\tanh\left(\frac{b_m + b_l}{2}\right)} \quad (66)$$

$$+ \sum_{k=1}^{N_1} \tanh\left(\frac{b_m - B_k}{2}\right) - \frac{\mathfrak{n}}{2} \sum_{k=1}^{N_1} \tanh\left(\frac{b_m + B_k}{2}\right) = f,$$

where the constant in the right-hand side reads:

$$f = \frac{1}{\nu} \left(1 + \frac{2c}{1-c} N\nu\right), \quad N = N_1 + N_2. \quad (67)$$

We shall study (65)-(66) for large crests, i.e. in the limit $N_1, N_2 \rightarrow \infty$. We expect that the poles B_1, \dots, B_{N_1} of the first pile (resp. b_1, \dots, b_{N_2} of the second pile) get condensed on a segment $J_1 = [B_{\min}, B_{\max}]$ (resp. $J_2 = [b_{\min}, b_{\max}]$) with a continuous nonnegative density $\varrho_1(B)$ (resp. $\varrho_2(b)$), as discussed in Section II. The densities are normalized as:

$$\int_{J_1} \varrho_1(B) dB = N_1, \quad \int_{J_2} \varrho_2(b) db = N_2. \quad (68)$$

and the flame slope (64) is retrieved as:

$$\phi_x(x) = \frac{-2\nu}{1-c} \text{Re} \left[\int_{J_1} \frac{\varrho_1(B') dB'}{\tan\left(\frac{x-iB'}{2}\right)} + \int_{J_2} \frac{\varrho_2(b') db'}{\tan\left(\frac{x-\pi-ib'}{2}\right)} \right] \quad (69)$$

The relations (65)-(66) then turn into coupled integral equations for the densities: for all $B \in J_1$,

$$\int_{J_1} \frac{\varrho_1(B') dB'}{\tanh\left(\frac{B-B'}{2}\right)} - \frac{\mathfrak{n}}{2} \int_{J_1} \frac{\varrho_1(B') dB'}{\tanh\left(\frac{B+B'}{2}\right)} \quad (70)$$

$$+ \int_{J_2} \frac{\varrho_2(b') db'}{\cotanh\left(\frac{B-b'}{2}\right)} - \frac{\mathfrak{n}}{2} \int_{J_2} \frac{\varrho_2(b') db'}{\cotanh\left(\frac{B+b'}{2}\right)} = f,$$

and for all $b \in J_2$:

$$\int_{J_2} \frac{\varrho_2(b') db'}{\tanh\left(\frac{b-b'}{2}\right)} - \frac{\mathfrak{n}}{2} \int_{J_2} \frac{\varrho_2(b') db'}{\tanh\left(\frac{b+b'}{2}\right)} \quad (71)$$

$$+ \int_{J_1} \frac{\varrho_1(B') dB'}{\cotanh\left(\frac{b-B'}{2}\right)} - \frac{\mathfrak{n}}{2} \int_{J_1} \frac{\varrho_1(B') dB'}{\cotanh\left(\frac{b+B'}{2}\right)} = f.$$

Even though $N \rightarrow \infty$, the full expression of f given in (67) is to be retained in (70)-(71). The reason why steady periodic fronts need an at least $O(N)$ actual-to-neutral wavelength ratio $1/\nu$ will be discussed in § IV F.

B. Reformulation by resolvents

To take advantage of the periodicity, we perform a first change of variable:

$$T = \frac{\tanh(B/2)}{\tanh(B_{\max}/2)}, \quad \tau = \frac{\tanh(b/2)}{\tanh(b_{\max}/2)}. \quad (72)$$

and define the resolvents for a complex variable z :

$$W_1(z) = \int_{\tilde{J}_1} \frac{\varrho_1(B(T)) dT}{z - T}, \quad W_2(z) = \int_{\tilde{J}_2} \frac{\varrho_2(b(\tau)) d\tau}{z - \tau}. \quad (73)$$

where $\tilde{J}_1 = [T_{\min}, 1]$ and $\tilde{J}_2 = [\tau_{\min}, 1]$ are the image of the supports after (72). The normalization conditions (68) are now rephrased as:

$$\begin{aligned} N_1 &= \int_{\tilde{J}_1} \frac{2 \tanh(B_{\max}/2) \varrho_1(B(T)) dT}{1 - \tanh^2(B_{\max}/2) T^2} \\ &= \oint_{\tilde{J}_1} \frac{dz}{2i\pi} \frac{2 \tanh(B_{\max}/2) W_1(z)}{1 - \tanh^2(B_{\max}/2) z^2}, \end{aligned} \quad (74)$$

and the contour of integration can be moved at infinity to pick up residues at $z = \pm 1$. Therefore:

$$N_1 = W_1\left(\frac{1}{\tanh(B_{\max}/2)}\right) - W_1\left(\frac{-1}{\tanh(B_{\max}/2)}\right). \quad (75)$$

The same computation holds for N_2 , with W_1 and B_{\max} replaced in (75) by W_2 and b_{\max} . Starting from the essential properties of resolvents emphasized in (25)-(26), the relations (70)-(71) can be transformed after a tedious algebra into a Riemann-Hilbert problem for W_i : for any $T \in \tilde{J}_1$,

$$\begin{aligned} W_1(T + i0) + W_1(T - i0) + \mathfrak{n} W_1(-T) \\ + 2W_2(1/PT) + \mathfrak{n} W_2(-1/PT) = \tilde{f}, \end{aligned} \quad (76)$$

and a symmetric equation for any $\tau \in \tilde{J}_2$,

$$\begin{aligned} W_2(\tau + i0) + W_2(\tau - i0) + \mathfrak{n} W_2(-\tau) \\ + 2W_1(1/P\tau) + \mathfrak{n} W_1(-1/P\tau) = \tilde{f}, \end{aligned} \quad (77)$$

where we have introduced the – yet unknown – constants:

$$P = \tanh(B_{\max}/2) \tanh(b_{\max}/2), \quad (78)$$

$$\tilde{f} = f - \frac{4c}{1-c} M, \quad (79)$$

$$\begin{aligned} M &= \int_{\tilde{J}_1} \frac{\tanh^2(B_{\max}/2) T \varrho_1(B(T)) dT}{1 - \tanh^2(B_{\max}/2) T^2} \\ &+ \int_{\tilde{J}_2} \frac{\tanh^2(b_{\max}/2) \tau \varrho_2(b(\tau)) d\tau}{1 - \tanh^2(b_{\max}/2) \tau^2}. \end{aligned} \quad (80)$$

C. Symmetric case

As of writing, we could not solve (76)-(77) in their full generality. Yet, we did determine the solution when

there is some symmetry between the two piles of poles, the same as for $c = 0$ [19], *viz.*:

$$\tilde{J}_1 = \tilde{J}_2 \equiv [r, 1] \text{ and } \varrho_1(B(T)) = \varrho_2(b(T)) \equiv \varrho(T). \quad (81)$$

This means that $\varrho_1(B)$ and $\varrho_2(b)$ can be deduced from one another by the rescaling encoded in (72). We stress that in general $\varrho_1(B) \neq \varrho_2(B)$, unless $B_{\max} = b_{\max}$, i.e. unless they have the same support (in which case (69) describes two copies of a monocoalesced periodic cell of length π). Likewise, the number of poles in each pile need not be equal. When (81) is satisfied, we obviously have $W_1(z) = W_2(z)$. The trick is now to introduce a new resolvent, which will incorporate simultaneously the terms involving z and $1/z$ in (76)-(77). For this purpose, we perform a second change of variable:

$$\eta = \frac{T}{1 + PT^2}, \quad (82)$$

already introduced in [20] to deal with the case $c = 0$, and which is invariant under $T \leftrightarrow 1/PT$. Though not invertible on the whole complex T -plane, (82) sends bijectively the support $[r, 1]$ of the density ϱ in the T -plane, to the segment:

$$\hat{J} = \left[\frac{r}{1 + Pr^2}, \frac{1}{1 + P} \right] \equiv [\eta_{\min}, \eta_{\max}] \quad (83)$$

in the η -plane. We can thus define:

$$\hat{\rho}(\eta) = \varrho(T(\eta)), \quad (84)$$

which is a density supported on \hat{J} , and next the resolvent for a complex variable z :

$$\hat{W}(z) = \int_{\hat{J}} \frac{\hat{\rho}(\eta) d\eta}{z - \eta}. \quad (85)$$

A computation shows that it is related to (73) by:

$$\hat{W}\left(\frac{z}{1 + Pz^2}\right) = W(z) + W(1/Pz) + \int_r^1 \frac{2PT \varrho(T) dT}{1 + PT^2}. \quad (86)$$

We deduce from (76) (or (77)) the relation, for all $\eta \in \hat{J}$:

$$\hat{W}(\eta + i0) + \hat{W}(\eta - i0) + \mathfrak{n} \hat{W}(-\eta) = \hat{f}. \quad (87)$$

The constant in the right hand-side combines (78) and the last term in (86), and becomes quite simple at the end:

$$\hat{f} = f - \frac{4c}{1-c} \hat{M}, \quad (88)$$

where

$$\begin{aligned} \hat{M} &= \int_{\hat{J}} \frac{S^2 \eta \hat{\rho}(\eta) d\eta}{1 - S^2 \eta^2} = \frac{1}{2} (\hat{W}(1/S) + \hat{W}(-1/S)), \\ S &= \tanh(B_{\max}/2) + \tanh(b_{\max}/2), \end{aligned} \quad (89)$$

and we have evaluated \hat{M} thanks to Cauchy residue formula. We now recognize an equation of the same type as

(27), hence solvable. The main difference with Section II is that the data of the number of poles N_1 and N_2 are encoded in a different way in the resolvent. We can rewrite (75) in terms of $\hat{\rho}$ only:

$$N_i = \int_j \left(S + \frac{\epsilon_i D}{\sqrt{1-4P\eta^2}} \right) \frac{\hat{\rho}(\eta)d\eta}{1-S^2\eta^2}, \quad i = 1, 2, \quad (90)$$

where $\epsilon_1 = +1$, $\epsilon_2 = -1$, and:

$$D = \tanh(B_{\max}/2) - \tanh(b_{\max}/2) \quad (91)$$

So, the total number of poles is retrieved in a simple way from \hat{W} :

$$N = \hat{W}(1/S) - \hat{W}(-1/S), \quad (92)$$

whereas the difference between the two piles is only given implicitly:

$$\frac{N_1 - N_2}{2} = \int_j \frac{D}{\sqrt{1-4P\eta^2}} \frac{\hat{\rho}(\eta)d\eta}{(1-S^2\eta^2)}. \quad (93)$$

Eventually, the flame slope (69) can be expressed directly in terms of the resolvent: if we first define

$$s(x) = \frac{\tan(x/2)}{\tanh(B_{\max}/2) - \tanh(b_{\max}/2) \tan^2(x/2)}, \quad (94)$$

we find after some algebra that:

$$\begin{aligned} \phi_x(x) &= -\frac{4\nu}{1-c} \int_j \frac{s(x) \hat{\rho}(\eta)d\eta}{\eta^2 + s^2(x)} \\ &= \frac{4\nu}{1-c} \text{Im}[\hat{W}(is(x))]. \end{aligned} \quad (95)$$

Before coming to the determination of $\phi_x(x)$, let us recapitulate the unknowns and the parameters for those symmetric solutions. Initially, the supports $[B_{\min}, B_{\max}]$ and $[b_{\min}, b_{\max}]$ of the pole densities in the first and second pile were unknown. The symmetric case we are studying amounts to consider supports with the same aspect ratio, namely:

$$r = \frac{\tanh(B_{\min}/2)}{\tanh(B_{\max}/2)} = \frac{\tanh(b_{\min}/2)}{\tanh(b_{\max}/2)}. \quad (96)$$

We are left with two unknowns, which can be encoded in the variables P and S defined in (78) and (89). On the other hand, c (or equivalently \mathbf{n} or γ), and the number of poles in each pile N_1 and N_2 , count as free parameters.

D. Solution for $0 < c < 1$

If we assume $B_{\min}, b_{\min} > 0$, we have $\eta_{\min} > 0$ (see (83)). We can repeat the analysis of Section III B. We first perform the change of variable

$$z = \eta_{\min} \text{sn}_k \psi, \quad k = \frac{\eta_{\min}}{\eta_{\max}} = \frac{(1+P)r}{1+Pr^2}, \quad (97)$$

and $\omega(\psi) = \hat{W}(z(\psi))$ can be extended as a holomorphic function of ψ in the whole complex plane. We deduce that $\eta_{\min} > 0$ implies $c > 0$, and the quantization condition:

$$\gamma K' = 2pK \quad \text{for some positive integer } p. \quad (98)$$

We already know that the positivity of the pole density requires $p = 1$. Besides, the general solution of (87) in terms of ω is obtained from (39), where $1/\nu$ (which appeared in the right-hand side of (27)) is replaced by \hat{f} given in (67) and (79). Exploiting the parametrization (9) of \mathbf{n} in terms of c , we arrive at:

$$\begin{aligned} \omega(\psi) &= \frac{f}{2+\mathbf{n}} + \frac{1}{2} [\omega(\psi_{1/S}) + \omega(-\psi_{1/S})] \\ &\quad + G \cosh[\pi(\gamma/2 + \psi/K')], \end{aligned} \quad (99)$$

where G is a constant to determine and $\psi_{1/S} = iK' + \delta$ with $0 < \delta < K$ is the unique point satisfying (97) for $z = 1/S$. This can be rephrased as:

$$\text{sn}_k(\delta) = \frac{S}{1+P} = \tanh\left(\frac{B_{\max} + b_{\max}}{2}\right). \quad (100)$$

We have a priori five unknowns: S, P, r as discussed in Section IV C, the constant G , and $\frac{1}{2}[\omega(\psi_{1/S}) + \omega(-\psi_{1/S})]$ (which is in fact irrelevant in the final result for the density and the flame slope) appearing in (99). We already have two normalization conditions (92)-(93) and the quantization condition (98). A fourth equation comes from the fact that $\hat{W}(\eta = \infty) = 0$ (see (85)), hence $\omega(iK') = 0$, and fixes the value of $\frac{1}{2}[\omega(\psi_{1/S}) + \omega(-\psi_{1/S})]$ in terms of the other unknowns. The fifth and last equation is obtained by consistency of (99): if we specialize to $\psi = \pm\psi_{1/S}$ and consider the half-sum of the two equations, we find:

$$-G \cosh(\pi\gamma/2) \cosh\left(\frac{\pi\delta}{K'}\right) = -\frac{f}{2+\mathbf{n}}. \quad (101)$$

Besides, (92) can be rewritten:

$$-2G \sinh(\pi\gamma/2) \sinh\left(\frac{\pi\delta}{K'}\right) = N. \quad (102)$$

Solving for G and $\psi_{1/S}$ in the system (101)-(102), and taking into account the expression (67) for f , yields:

$$G = -\frac{F}{4\nu} \frac{(1-c)^{3/2}}{c}, \quad F = \sqrt{1 + \frac{4c}{1-c} N\nu(1-N\nu)}, \quad (103)$$

and:

$$\frac{S}{1+P} = \text{sn}_k \left[\frac{K'}{\pi} \tanh^{-1} \left(\frac{2N\nu\sqrt{c}}{1-c(1-2N\nu)} \right) \right]. \quad (104)$$

Then, the system of equations (93),(98),(104) determines implicitly S, P and r in terms of N_1, N_2 and c , and it can be solved at least numerically. The final answer for the reduced density of poles (81),(84) reads:

$$\hat{\rho}(\eta) = \frac{1}{2\pi} \sqrt{\frac{1-c}{c}} \frac{F}{\nu} \sin[\pi\chi(\eta)], \quad (105)$$

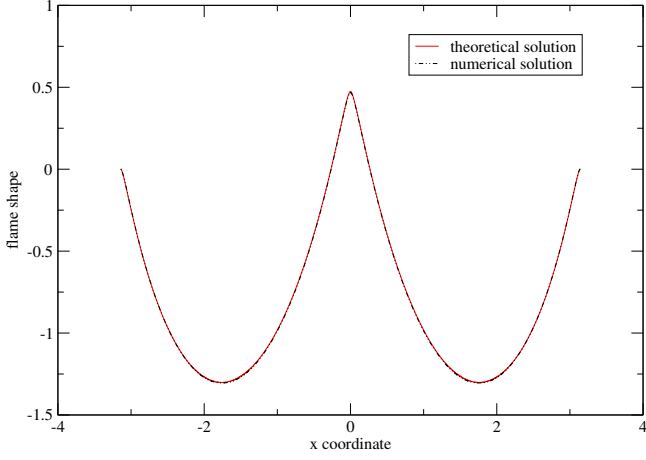


FIG. 4. Bicoalesced periodic front shape $\phi(x)$ with $c > 0$. The plot assumes $(N_1, N_2) = (200, 100)$, $1/\nu = 600.5$ and $c = 0.5$. We display the comparison between the numerical resolution of (65)-(66) and integration of the theoretical formula (107).

where we have introduced:

$$\chi(\eta) = \frac{1}{K'} \text{nd}_{k'}^{-1} \left(\frac{1 + Pr^2}{r} \eta \right), \quad k' = \sqrt{1 - k^2}. \quad (106)$$

And from (95), we deduce the flame slope:

$$\phi_x(x) = -\frac{F}{\sqrt{c}} \sin \left[\frac{\pi}{K'} \text{sc}_{k'}^{-1} \left(\frac{(1 + Pr^2)}{r} s(x) \right) \right], \quad (107)$$

where $s(x)$ and F were defined in (94) and (103). A flame shape $\phi(x)$ corresponding to (107) is plotted in Fig. 4.

E. Solution for $-1 < c < 0$

In this regime, we must have $B_{\min} = b_{\min} = 0$, i.e. $\eta_{\min} = 0$ or equivalently $r = 0$, and we can repeat the analysis of Section III C. We first perform the change of variable:

$$z = \frac{\eta_{\max}}{\cosh \psi}, \quad (108)$$

the function $\omega(\psi) = \hat{W}(z(\psi))$ can be extended as a holomorphic function in the whole ψ -plane, and has the general expression (55) where $1/\nu$ is replaced – as in Section IV D – by the appropriate constant term:

$$\omega(\psi) = \frac{f}{2 + \mathbf{n}} + \frac{1}{2} [\omega(\psi_{1/S}) + \omega(i\pi - \psi_{1/S})] + G \cosh[\gamma(\psi - i\pi)], \quad (109)$$

where G is some constant to determine, and $\psi_{1/S} = i(\pi/2 - \delta)$ with $0 < \delta < \pi/2$ is the unique point satisfying (108) for $z = 1/S$. In other words:

$$\sin(\delta) = \frac{S}{1 + P} = \tanh \left(\frac{B_{\max} + b_{\max}}{2} \right). \quad (110)$$

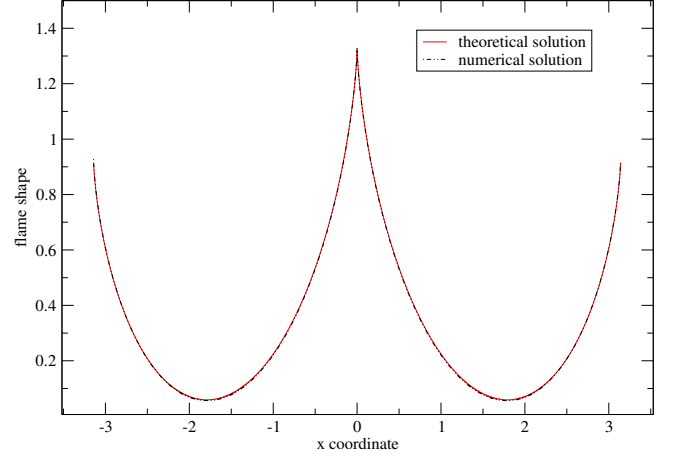


FIG. 5. Bicoalesced periodic front shape $\phi(x)$ with $c < 0$. The plot assumes $(N_1, N_2) = (200, 100)$, $1/\nu = 600.5$ and $c = -0.25$. We display the comparison between the numerical resolution of (65)-(66) and integration of the theoretical formula (114).

Since the discussion to determine the unknowns is also very similar to Section IV D, we only give the results:

$$G = -\frac{F}{4\nu} \frac{(1 - c)^{3/2}}{-c} \quad (111)$$

with the same constant F appearing in (103), and:

$$\frac{S}{1 + P} = \sin \left[\frac{1}{\gamma} \tan^{-1} \left(\frac{2N\nu\sqrt{-c}}{1 - c(1 - 2N\nu)} \right) \right]. \quad (112)$$

Together with the implicit relation (93), Eq. (112) fixes S and P , and thus the solution of our problem. The final result for the reduced density of poles (81),(84) reads:

$$\hat{\rho}(\eta) = \frac{1}{2\pi} \sqrt{\frac{1 - c}{-c}} \frac{F}{\nu} \sinh \left[\gamma \cosh^{-1} \left(\frac{1}{(1 + P)\eta} \right) \right], \quad (113)$$

and the corresponding flame slope is:

$$\phi_x(x) = -\frac{F}{\sqrt{-c}} \sinh \left[\gamma \sinh^{-1} \left(\frac{1}{(1 + P)s(x)} \right) \right], \quad (114)$$

where $s(x)$ and F were defined in (78) and (103). As expected, the resulting expression for $\phi_x(x)$ is symmetric under $(x, B_{\max}) \leftrightarrow (x - \pi, b_{\max})$. A flame shape $\phi(x)$ corresponding to (114) is plotted in Fig. 5.

F. Discussion

As is patent on comparing (113)-(114) with (105)-(107), using $-1 < c < 0$ instead of $0 < c < 1$ again merely amounts to selecting the relevant expression of γ , and to replacing the elliptic functions by suitable hyperbolic ones, in the pole density and flame slope. Both

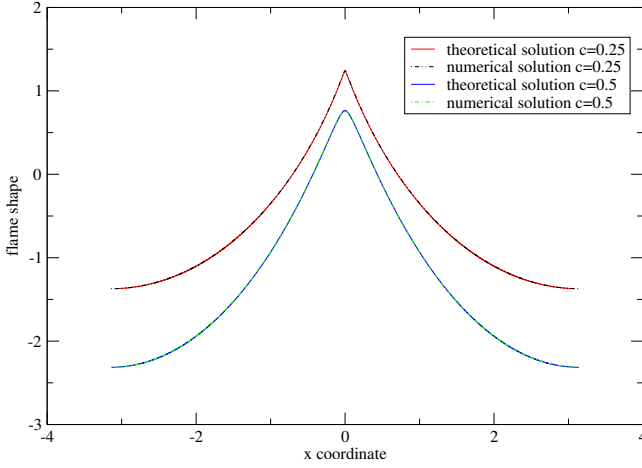


FIG. 6. Monocoalesced periodic front shapes $\phi(x)$ with $c > 0$. The plots assume $(N_1, N_2) = (100, 0)$ and $1/\nu = 199.5$. For the two values $c = 0.25$ (top) and $c = 0.5$ (bottom), we show the comparison between the numerical resolution of (65)-(66) and integration of the theoretical formula (107).

situations thus share several trends, which are appropriate to discuss first.

Since $\text{sn}_k(K) = 1 = \sin(\pi/2)$, $B_{\max} + b_{\max} \rightarrow \infty$ follows in the limit $2\nu N \rightarrow 1$, from (97), (100) and (104) if $0 < c < 1$, or (110) and (112) if $-1 < c < 0$. Next, (93) indicates that only the uppermost end of the most populated pile (namely, B_{\max} if $N_1 > N_2$) actually goes to infinity in either case; since B_{\max} cannot go further vertically, steady bicoalesced periodic patterns cannot support an arbitrary large number of poles per wavelength [18], just like when $c = 0$ [17, 19]. This can be traced back to (65)-(66), for example with $b_{N_2} < B_{N_1} \rightarrow \infty$ if $N_1 > N_2$, in which limit the condition

$$N = N_1 + N_2 = N_{\text{opt}}(\nu) = \lfloor \frac{\nu + 1}{2\nu} \rfloor \quad (115)$$

is obtained. Note that $N_{\text{opt}}(2\nu) \leq N_{\text{opt}}(\nu)/2$, but the difference is asymptotically small for large wrinkles, as $2\nu N_{\text{opt}}(\nu) \sim 1$ for $\nu \rightarrow 0^+$. Conversely, a large actual-to-neutral wavelength ratio $1/\nu \geq (2N - 1)$ is required for a total population of $2N$ bicoalesced poles to stay steady "in" a cell.

The analysis of Section IV of the large steady wrinkles governed by the ZT equation (1) contain as limiting cases all the results available so far. Monocoalesced 2π -periodic cells correspond to $2\nu N_2 \rightarrow 0$ at fixed νN_1 (see Fig 6). In the present continuous approximation of the pole equations, b_{\max} then vanishes and this amounts to replacing:

$$\frac{1}{(1+P)\eta} \rightarrow \frac{\tanh(B_{\max}/2)}{\tanh(B/2)}, \quad \frac{1}{(1+P)s(x)} \rightarrow \frac{\tanh(B_{\max}/2)}{\tan(x/2)}, \quad (116)$$

in (113) and (114) respectively. For such two-crested

periodic patterns, $\frac{\tanh(B_{\max}/2)}{\tan(x/2)}$ plays the part $\frac{B_{\max}}{x}$ did for isolated crests, see (44)-(47) and (59)-(60). Also, if $-1 < c < 0$, (112)-(114) then resume the expressions found in [19]. The isolated crests constitute a further degeneration of (116) and formally corresponds to $2\nu N_1 \ll 1$ and restricting oneself to a region of the complex plane where $|x + iB| = O(N_1\nu) \ll 1$. Then $B_{\max} = O(N_1\nu) \ll 1$ by (100) or (110),

$$\frac{1}{(1+P)\eta} \rightarrow \frac{B_{\max}}{B}, \quad \frac{\tanh(B_{\max}/2)}{\tan(x/2)} \rightarrow \frac{B_{\max}}{x}, \quad (117)$$

in (116), the prefactor F defined in (103) goes to 1, and the density and the flame slope reduce to (44)-(47) or (59)-(60).

For equally populated piles of poles (i.e. $N_1 = N_2$), we have $b_{\max} = B_{\max}$, whence (82) and (94) simplify to:

$$\frac{1}{(1+P)s(x)} = \frac{\tanh B_{\max}}{\tan x}, \quad \frac{1}{(1+P)\eta} = \frac{\tanh B_{\max}}{\tanh B}. \quad (118)$$

The comparison with (116) shows that (118) describes two copies of a monocoalesced cell of wavelength π : this was actually expected from the outset in view of the discrete pole equations (65)-(66) with $N_1 = N_2$, since $\tanh(a) + \frac{1}{\tanh(a)} = \frac{2}{\tanh(2a)}$.

The main qualitative difference between the $c \leq 0$ and $c > 0$ cases undoubtedly is about the tips of large front wrinkles. Even when $N_{1,2} \rightarrow \infty$ (and keeping $\nu N_{1,2} = O(1)$), these are smooth maxima of $\phi(x)$ if $c > 0$, with $O(B_{\min})$ radii of curvature that quickly increase with c if $0 < c \ll 1$ (see Fig. 6-4), and are sharp cusps otherwise (see Fig. 5). Specifically, the centered tips locally have $\phi_x(x) \propto -\text{sgn}(x)|x|^{-\alpha}$ and thus

$$\phi(x) - \phi(0) \propto -|x|^{1-\alpha}, \quad \alpha = \frac{2}{\pi} \tanh^{-1}(\sqrt{-c}). \quad (119)$$

with $0 < \alpha < 1/2$ for $-1 < c < 0$. The MS value $c = 0$ is marginal and was already known to give logarithmic cusps [17, 19]. While affecting the crests ($-\mathcal{H}[\phi_x] > 0$), the value of c also modifies the front troughs (minima of $\phi(x)$, where $\mathcal{H}[\phi_x] > 0$), but differently. This can be qualitatively understood from (1), by transferring the nonlocal nonlinearity $c\mathcal{H}[\phi_x]^2$ to the right-hand side: if $c < 0$, the resulting "effective driving term" of instability, $-\mathcal{H}[\phi_x](1 + \frac{c}{2}\mathcal{H}[\phi_x])$, is reduced (or enhanced) at troughs (or crests) compared to its MS counterpart alone and tends to render them rounder (or sharper); $c > 0$ has opposite influences.

And, importantly again, whatever the value of $-1 \leq c < 1$ is, the analytical predictions of Section IV perfectly agree with the numerical resolutions of (65)-(66) for the discrete poles B_k and b_m , and with the bicoalesced front slopes ensuing from (64) and numerical quadrature. In particular, $\phi(x)$ is found for $c > 0$ to have 4 inflexion points whenever $N_1/N_2 \neq 0, \infty$ (see Fig. 4), and only 2 inflexion points otherwise; in either case, $\max|\phi_x(x)| = \frac{F}{\sqrt{c}}$ is the same at all of them and only depends on $c > 0$ and $N\nu$.

V. CONCLUSION

We have investigated with complex analysis methods solutions of the ZT equation with free parameter $-1 < c < 1$, describing stationary flame shapes in the limit of large wrinkles. We rederived the known expression (60) for a front with an isolated crest when $-1 < c < 0$, and obtained its counterpart (47) in the regime $0 < c < 1$. We also obtained new expressions describing bicoalesced, space-periodic fronts with some symmetry (see § IV C) in the regime $0 < c < 1$ (107) or $-1 < c < 0$ (114), which are in agreement with numerical simulations (resp. Fig. 4 and Fig. 5). The results obtained in the limit case of monocoalesced periodic fronts are also new (see Section IV F, and Fig 6 for comparison to numerics).

The preceding analyses do not exhaust all the theoretical problems as to (1), for it admits even more general solutions than the symmetric bicoalesced ones studied in Section IV. For example, the so-called *interpolating solutions* [32, 34] are still awaiting for detailed descriptions. Their existence can be inferred on noticing that, besides $2N$ bicoalesced poles vertically aligned at $x = 0$ or $x = \pi$, N_∞ extra pairs may stay in equilibrium at $Z_k = \pm i\infty + \frac{(2k-1)\pi}{N_\infty}$ for $k = 1, \dots, N_\infty$ if $0 \leq 2\nu N = 1 - \nu N_\infty < 1$; with $2\nu N$ being further reduced, the N_∞ remote poles will move and be located at finite $\text{Im } Z_k$ [32, 34]. Although such solutions are likely unstable (as in the $c = 0$ case), their computation in the limit $\nu \rightarrow 0^+$ and still $\nu N_{1,2,\infty} = O(1)$ with similar methods is under investigation. As another example, space-periodic configurations with more than 2 unequal piles per cell certainly exist if ν is small: a single pair of poles may already stay in equilibrium near the trough of a base front if wide enough, thereby creating an incipient extra crest there [19]. Whether this is within reach of resolvent approaches when the extra poles get many constitutes a challenge still to be met, as some of the poles would again condense on curved arcs in such configurations.

In the continuous description of, say, isolated crests, ν could have been absorbed in the normalization of the pole density, since the flame slopes (60) or (47) only depend on ν and N through the combination $\mathcal{N} = \nu N$. This parameter \mathcal{N} could then be *any positive real number*, labeling a continuum of solutions. Without invoking pole decompositions, can one retrieve the selection of a discrete set of solutions (e.g. requiring $N = \mathcal{N}/\nu$ to be an integer) if small curvature effects ($0 < \nu \ll 1$) are restored afterward? This was answered in the affirmative for viscous fingering or needle-crystals [35]: quantization then resulted from a solvability condition on short-scale steady front-shape perturbations (local wavenumbers of order $1/\nu$). The corresponding procedure for flames has so far not been provided, and would be tantamount to performing directly a WKB analysis in (20).

A related matter concerns the solutions with integer $p > 1$ first encountered in § III B but discarded to ensure positivity of the pole density. We have shown in § II C

that they nonetheless lead to solutions of the "inviscid ZT equation", i.e. (1) without the $\nu\phi_{xx}$ term. The $p > 1$ oscillating $\phi_x(x)$ profiles obtained for $0 < c < 1$ could then be viewed as steady nonlinear perturbations of the $p = 1$ solution (47), in a way reminiscent of what happens in needle-crystal growth [35].

Besides, other equations than (1) may reduce to the inviscid ZT form in the large wrinkle limit, at least outside the cusps they might have. In case the same outer profiles as described by (59)-(60) would apply, one would need to determine the appropriate \mathcal{N} that enters in B_{\max} in such equations as (57). One may guess that the inner front tip structure yields \mathcal{N} (e.g., by matching), and one may wonder whether its value is quantized.

We also argued (the details are found in Appendix C) that the ZT equation in the form (20) appears in the β -deformation of the $\mathcal{O}(n)$ random matrix model (C1), in the limit of large matrices. One may wonder whether this very matrix model for finite N (and its generalization where the eigenvalue lives in a certain region of the complex plane) could provide itself a statistical-mechanical description of a combustion problem.

Appendix A: The $c \rightarrow 1^-$ limit

The then strong coupling between B_k of unlike signs in (5) makes the pole population split in two groups, separated by a distance of about $2h \geq \nu \frac{1+c}{1-c}$ that will exceed the width of each group for $c \rightarrow 1^-$. With $B_{j<0} \approx -h$ to leading order, (6) written for B_1, \dots, B_N simplifies to:

$$\sum_{\substack{j=1 \\ j \neq k}}^N \frac{2\nu}{(B_k + h) - (B_j + h)} + 2 \frac{1+c}{1-c} \frac{\nu N}{B_k + h} \approx 1. \quad (\text{A1})$$

According to Stieltjes (see [36], the review [22] and references therein), the solutions $\xi_k = \frac{B_k + h}{\nu}$ to (A1) are the zeros of the associated Laguerre polynomial $\mathcal{L}_N^{(\alpha)}(\xi)$, with $\alpha = -1 + 2N \frac{1+c}{1-c}$. One may select h so that $\sum_{j=1}^N \frac{1}{B - (-B_j)} \approx \frac{N}{B+h}$ be exact at $B = h$, whereby $\frac{h}{\nu} = \frac{\alpha+1}{2} = N \frac{1+c}{1-c}$; whatever N is, $B_N - B_1 \propto \frac{\nu N}{\sqrt{1-c}}$ [37] is asymptotically smaller than $h \sim \frac{2\nu N}{1-c}$ when $c \rightarrow 1^-$, as anticipated. If next $N \rightarrow \infty$, the zeros of $\mathcal{L}_N^{(\alpha)}(\eta)$ are distributed according to a Marčenko-Pastur density [38]

$$\rho(\eta) \propto \frac{\sqrt{(\xi_{\max} - \xi)(\xi - \xi_{\min})}}{\xi}, \quad (\text{A2})$$

with $\xi_{\max/\min} = N(2 + a \pm 2\sqrt{1+a})$ and $a = \lim_{N \rightarrow \infty} \frac{\alpha}{N} \approx 2 \frac{1+c}{1-c}$. The ensuing pole density $\rho(B)$ is nonzero only for $B_{\min} < |B| < B_{\max}$, with $B_{\max(\min)} \approx \nu \xi_{\max(\min)} - h > 0$.

Appendix B: Origin of the quantization (37)

We first recall the definition of the first Jacobi theta function:

$$\vartheta_1(w|\tau) = i \sum_{m \in \mathbb{Z}} (-1)^m e^{i\pi(2m-1)w} e^{i\pi\tau(m+1/2)^2}. \quad (\text{B1})$$

This series is absolutely convergent whenever the parameter τ has positive imaginary part, it defines an entire function of $w \in \mathbb{C}$ with the following properties:

$$\vartheta_1(w+1|\tau) = -\vartheta_1(w|\tau), \quad (\text{B2})$$

$$\vartheta_1(w+\tau|\tau) = -e^{-i\pi(2w+\tau)} \vartheta_1(w|\tau), \quad (\text{B3})$$

$$\vartheta_1(w=0|\tau) = 0. \quad (\text{B4})$$

Therefore, we may build a function ω_+ satisfying (36) with a ratio of theta functions. The choice of ω_+ is arbitrary: indeed, the ratio of two functions satisfying (36) is $2K$ - and $2iK'$ -periodic, so that it can be absorbed in the choice of $g(\psi)$ in (35). In this appendix, we take:

$$\omega_+(\psi) = \frac{\vartheta_1\left(\frac{\psi}{2iK'} - i\gamma/2|\tau\right)}{\vartheta_1(z|\tau)}, \quad \tau = \frac{iK}{K'}. \quad (\text{B5})$$

This function has a simple pole at $\psi = 0$ and a simple zero at $\psi = -\gamma K'$ (modulo the translations by $2K$ and $2iK'$), unless:

$$\gamma K' = 2Kp \quad \text{for some integer } p. \quad (\text{B6})$$

We are now in position to explain why the case considered in § III B imposes the quantization condition (B6). Since the right-hand side in (27) was a constant, we were looking for a *entire* function $\omega(\psi)$. The latter was decomposed as (35), hence:

$$g(\psi)\omega_+(\psi) = \frac{e^{\pi\gamma}\omega(\psi+2K) - \omega(\psi)}{e^{2\pi\gamma} - 1} - \frac{e^{\pi\gamma} - 1}{e^{2\pi\gamma} - 1} \frac{f}{2 + \mathbf{n}} \quad (\text{B7})$$

is also an entire function (we recall the assumption $c \neq 0$, thus $\gamma > 0$). When (B6) is not satisfied, the choice of (B5) would imply that $g(\psi)$ has a simple pole at $\psi = -\gamma K'$, and no other singularity in \mathbb{C} . But no such function exists, because the total order of poles (modulo translations) of a meromorphic doubly-periodic function is at least 2. The quantization (B6) was thus necessary for our problem to admit solutions.

Appendix C: $\mathcal{O}(\mathbf{n})$ matrix models and ZT equation

Let us consider the statistical ensemble of N particles at position B_1, \dots, B_N on the positive real axis, distributed according to the measure:

$$\prod_{i=1}^N dB_i e^{-\beta\mathcal{V}(B_i)/2} \times \frac{\prod_{1 \leq i < j \leq N} |B_i - B_j|^\beta}{\prod_{1 \leq i, j \leq N} (B_i + B_j)^{\mathbf{n}\beta/4}}, \quad (\text{C1})$$

where $\mathcal{V}(B)$ is a given, smooth function. For $\beta = 2$, this is the $\mathcal{O}(\mathbf{n})$ model introduced by [25, 26] in relation with

the problem of counting configurations of self-avoiding loops on random discrete surfaces. This model has been studied intensively since then [27, 28, 39, 40], and also appears in the context of quantum entanglement [41]. When $\beta = 2$ and \mathbf{n} is an integer, (C1) is the measure induced on eigenvalues B_1, \dots, B_N of a random hermitian, positive definite matrix \mathbf{B} , and coupled to \mathbf{n} other hermitian matrices $\mathbf{A}_1, \dots, \mathbf{A}_\mathbf{n}$ with a joint distribution:

$$d\mathbf{B} \prod_{j=1}^{\mathbf{n}} d\mathbf{A}_j e^{-\text{Tr}[\mathcal{V}(\mathbf{B}) + \sum_{j=1}^{\mathbf{n}} \mathbf{B}\mathbf{A}_j^2]}. \quad (\text{C2})$$

The quantity $\Delta(\mathbf{z})^2 = \prod_{i < j} |z_i - z_j|^2$ is characteristic of the eigenvalue distribution of random hermitian matrices whose full distribution is invariant under conjugation by a unitary matrix: it expresses the repulsion between eigenvalues of such a matrix taken at random. The product in the denominator of (C1) arises from the integration over the matrices \mathbf{A}_j (which have a Gaussian distribution according to (C2)). In random matrix theory, (C2) is called "the $\mathcal{O}(\mathbf{n})$ matrix model", and replacing $\Delta(\mathbf{z})^2$ by $\Delta(\mathbf{z})^\beta$ is the " β -deformation".

In this model, the B_k are random. We can define again a resolvent as an expectation value against the measure (C1):

$$W(z) = \left\langle \sum_{i=1}^N \frac{1}{z - B_i} \right\rangle, \quad (\text{C3})$$

We claim that, when N is large and with the choice $\mathcal{V}(B) = B/\nu$, $W(z)$ satisfies an equation like (20), which amounts to saying that $\phi_x(x) = \frac{4\nu}{1-c} \text{Im}[W(ix)]$ is solution of a ZT equation (see § II C).

It is convenient to introduce the two-points resolvent:

$$W(z_1, z_2) = \left\langle \sum_{j,k=1}^N \frac{1}{z_1 - B_j} \frac{1}{z_2 - B_k} \right\rangle. \quad (\text{C4})$$

In general $W(z_1, z_2) \neq W(z_1)W(z_2)$. However, when N becomes large, the random B_k for $k = 1, \dots, N$ are distributed in a deterministic way, with some density $\varrho(B)$ supported on \mathcal{C} . Hence:

$$W(z_1, z_2) \sim W(z_1)W(z_2) \quad \text{when } N \rightarrow \infty. \quad (\text{C5})$$

Using integration by parts, one can derive the Schwinger-Dyson relations valid for any N [40]:

$$W(z, z) + W(-z, -z) + \mathbf{n}W(z, -z) + \left(\frac{2}{\beta} - 1\right) [W'(z) + W'(-z)] - \frac{1}{\nu} [W(z) + W(-z)] = 0. \quad (\text{C6})$$

This can be simplified when N is large owing to (C5):

$$W(z)^2 + W(-z)^2 + \mathbf{n}W(z)W(-z) + \left(\frac{2}{\beta} - 1\right) [W'(z) + W'(-z)] - \frac{1}{\nu} [W(z) + W(-z)] = 0. \quad (\text{C7})$$

which coincides, up to the rescaling $z \rightarrow \frac{z}{2/\beta - 1}$, with (20).

-
- [1] G. Darrieus, (1938), work presented at La Technique Moderne, Paris, unpublished.
- [2] L. Landau, *Acta Physicochim. URSS* **19**, 77 (1944).
- [3] G. Markstein, *J. Aeronaut. Sci.* **18**, 199 (1951).
- [4] P. Pelcé and P. Clavin, *J. Fluid Mech.* **124**, 219 (1982).
- [5] F. Creta and M. Matalon, *J. Fluid. Mech.* **680**, 225 (2011).
- [6] G. Sivashinsky, *Acta Astron.* **4**, 1177 (1977).
- [7] D. Michelson and G. Sivashinsky, *Acta Astron.* **4**, 1207 (1977).
- [8] F. Röpke, W. Hillebrandt, and J. Niemeyer, *Astron. Astrophys.* **420**, 411 (2004), [astro-ph/0312092](#).
- [9] P. Clavin and G. Sivashinsky, *J. Phys. France* **48**, 193 (1987).
- [10] K. Kazakov and M. Liberman, *Phys. Fluids* **14**, 1166 (2002), [physics.flu-dyn/0106076](#).
- [11] K. Kazakov, *Phys. Fluids* **17** (2005), 032107, [physics.flu-dyn/0407044](#).
- [12] K. Kazakov, O. Peil, and N. Pekal'n, In preparation.
- [13] S. Zhdanov and B. Trubnikov, *J. Exp. Theor. Phys.* **68**, 65 (1989).
- [14] V. Bychkov, K. Kovalev, and M. Liberman, *Phys. Rev. E* **60**, 2897 (1999).
- [15] J. Quinard, G. Searby, B. Denet, and J. Grana-Otero, *Flow, Turbulence and Combustion* (2011), [dx.doi.org/10.1007/s10494-011-9350-3](#).
- [16] D. Vaynblatt and M. Matalon, *Siam J. Appl. Math.* **60**, 679 (2000).
- [17] O. Thual, U. Frisch, and M. Hénon, *J. Phys. France* **46**, 1485 (1985).
- [18] G. Joulin, *J. Exp. Theor. Phys.* **100**, 428 (1991).
- [19] G. Joulin and B. Denet, *Phys. Rev. E* **78** (2008), 016315, [physics.class-ph/0806.4338](#).
- [20] G. Joulin and B. Denet, *Phys. Lett. A* **376**, 1797 (2012), [nlin.PS/1204.6565](#).
- [21] C. Dunkl, *Indagationes Mathematicae* **88**, 147 (1985).
- [22] F. Marcellán, A. Martínez-Finkelshtein, and P. Martínez-González, *J. Comp. Appl. Math.* **207**, 258 (2007), [math.CA/0512293](#).
- [23] P. Deift, *Orthogonal polynomials and random matrices : a Riemann-Hilbert approach* (AMS, New York, 1998) Courant Institute of Mathematical Sciences.
- [24] P. Forrester, *Log-gases and random matrices*, London Mathematical Society Monographs (Princeton University Press, Princeton, 2010).
- [25] M. Gaudin and I. Kostov, *Phys. Lett. B* **220** (1989).
- [26] I. Kostov, *Mod. Phys. Lett. A* **4**, 217 (1989).
- [27] B. Eynard and C. Kristjansen, *Nucl. Phys. B* **455**, 577 (1995), [hep-th/9506193](#).
- [28] B. Eynard and C. Kristjansen, *Nucl. Phys. B* **466**, 463 (1996), [hep-th/9512052](#).
- [29] E. Titchmarsh, *Introduction to the theory of Fourier integrals* (Clarendon Press, Oxford, 1937).
- [30] D. Guo and Z. Wang, *Special functions* (World Scientific, Singapore, 1989).
- [31] E. Whittaker and G. Watson, *A course of modern analysis*, Cambridge Mathematical Library (1996) 4th edition.
- [32] B. Denet, *Phys. Rev. E* **74** (2006), 036303, [physics.class-ph/0604120v1](#).
- [33] O. Travnikov, V. Bychkov, and M. Liberman, *Phys. Rev. E* **61**, 468 (2000).
- [34] L. Guidi and D. Marchetti, *Phys. Lett. A* **308**, 162 (2003).
- [35] P. Pelcé, *Théorie des formes de croissance: digitations, dendrites et flammes*, *Savoirs actuels* (EDP Sciences, Paris, 2000).
- [36] G. Szegő, *Orthogonal polynomials* (Amer. Math. Soc., 1939) reprinted with corrections (2003).
- [37] M. Ismail and X. Li, *Am. Math. Soc.* **115** (1992), 0002-9939.
- [38] V. Marčenko and L. Pastur, *Math USSR-Sbornik* **1**, 457 (1967).
- [39] I. Kostov and M. Staudacher, *Nucl. Phys. B* **384**, 459 (1992), [hep-th/9203030](#).
- [40] G. Borot, (2011), Thèse de doctorat, Université d'Orsay. [math-ph/1110.1493](#).
- [41] G. Borot and C. Nadal, *J. Phys. A: Math. Theor.* **45** (2012), 075209, [cond-mat.stat-mech/1110.3838](#).